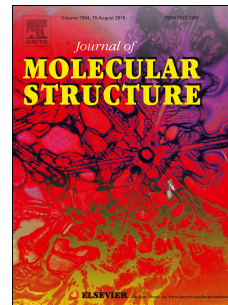


Accepted Manuscript

Synthesis, structural characterization and theoretical studies of a new Schiff base 4-(((3-(*tert*-Butyl)-(1-phenyl)pyrazol-5-yl) imino)methyl)phenol

Fernando Cuenú, Jennifer Londoño-Salazar, John Eduard Torres, Rodrigo Abonia, Richard F. D'Vries



PII: S0022-2860(17)31276-0

DOI: [10.1016/j.molstruc.2017.09.078](https://doi.org/10.1016/j.molstruc.2017.09.078)

Reference: MOLSTR 24327

To appear in: *Journal of Molecular Structure*

Received Date: 2 August 2017

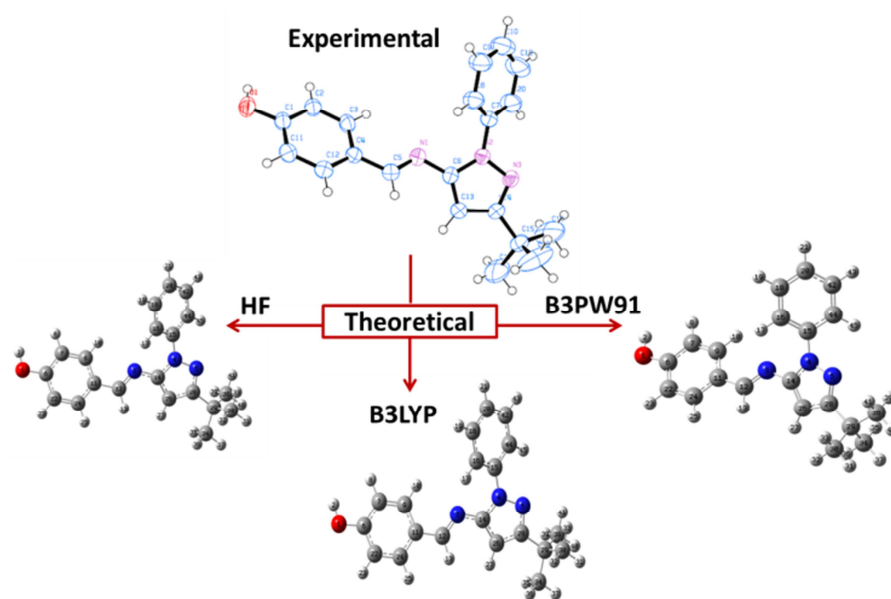
Revised Date: 19 September 2017

Accepted Date: 21 September 2017

Please cite this article as: F. Cuenú, J. Londoño-Salazar, J.E. Torres, R. Abonia, R.F. D'Vries, Synthesis, structural characterization and theoretical studies of a new Schiff base 4-(((3-(*tert*-Butyl)-(1-phenyl)pyrazol-5-yl) imino)methyl)phenol, *Journal of Molecular Structure* (2017), doi: 10.1016/j.molstruc.2017.09.078.

This is a PDF file of an unedited manuscript that has been accepted for publication. As a service to our customers we are providing this early version of the manuscript. The manuscript will undergo copyediting, typesetting, and review of the resulting proof before it is published in its final form. Please note that during the production process errors may be discovered which could affect the content, and all legal disclaimers that apply to the journal pertain.

Graphical abstract



Synthesis, Structural Characterization and Theoretical Studies of a new Schiff Base 4-(((3-(*tert*-Butyl)-(1-phenyl)pyrazol-5-yl)imino)methyl)phenol

Fernando Cuenú^{a*}, Jennifer Londoño-Salazar^a, John Eduard Torres^a, Rodrigo Abonia^b, Richard F. D'Vries^c

^a Laboratorio de Química Inorgánica y Catálisis, Programa de Química, Universidad del Quindío, Carrera 15, Calle 12 Norte, Armenia, Colombia

^b Departamento de Química, Universidad del Valle, AA 25630, Cali-Colombia

^c Universidad Santiago de Cali, Calle 5 # 62-00, Cali, Colombia

*Corresponding author. Laboratorio de Química Inorgánica y Catálisis, Programa de Química, Universidad del Quindío, Carrera 15, Calle 12 Norte, Armenia-Colombia. Mail: fercuenu@uniquindio.edu.co

ABSTRACT

4-(((3-(*tert*-Butyl)-(1-phenyl)pyrazol-5-yl)imino)methyl)phenol (**4-OHFPz**) was synthesized and characterized by FT-IR, MS, NMR, and single-crystal X-ray diffraction. Optimization of molecular geometry, vibrational frequencies, and chemical shifts were calculated by using the methods of density functional theory (DFT) with B3LYP and B3PW91 as functionals and Hartree-Fock with 6-311G++(d,p) as basis set using the GAUSSIAN 09 program package. With the VEDA 4 software, the vibrational frequencies were assigned in terms of the potential energy distribution (PED). The equilibrium geometries calculated by all methods were compared with X-ray diffraction results, indicating that the theoretical results matches well with the experimental ones. The data obtained from the vibrational analysis and the calculated NMR are consistent with the experimental spectra.

KEYWORDS: Schiff bases, Pyrazole, DFT, Hartree-Fock, NMR, FT-IR.

1. Introduction

Schiff bases are an important class of organic compounds with significant biological and chemical activities. Several Schiff base bearing *N*-heterocyclic groups in their structures have received much attention in biological processes because they have shown a number of properties like antimicrobial [1], antifungal [2], antituberculous [3], antitumoral [4], antiparasitic [5] and antiviral [6] activity. They also have been considered as useful synthetic building blocks in coordination chemistry because of their chelating effects [7].

Regarding to our interest in developing new structures from pyrazole derivatives, the new Schiff base (**4-OHFPz**) was synthesized because of imines and pyrazole compounds have chemical and biological properties, also **4-OHFPz** will later be coordinated to palladium. This Pd-Schiff base complex will be evaluated in C-C coupling reactions as well as potential antifungal and anticancer agents. The crystal structure, the vibrational and electronic spectra are reported in this work. The vibrational frequencies and the geometric parameters of the compound mentioned in the ground state were calculated by *ab initio* (HF) and DFT (B3LYP, B3PW91) methodologies with the standard basis set 6-311G++(d,p). A detailed interpretation of the vibrational spectrum of the aforementioned compound was made on the basis of the calculated potential energy distribution (PED). The ^1H and ^{13}C NMR spectra were calculated with *ab initio* and DFT by the GIAO method from the optimized geometries, with tetramethylsilane (TMS) as standard and DMSO as solvent. To calculate the HOMO and LUMO energies and the absorption spectrum, the TD-SCF (Time-dependent self-consistent field) method was used by using the structure optimized with the basis set 6-311G++ (d, p) in acetonitrile as solvent.

2. Experimental

2.1. Analytical and physicochemical measurements

Synthesis of **4-OHFPz** was monitored by thin-layer chromatography (TLC) using silica gel plates 60 F254 (Merck), visualization was achieved by ultraviolet (UV) light. Melting points were determined on a Büchi melting point apparatus. Infrared spectra were taken on a Perkin Elmer FT 2000 series spectrophotometer using KBr disks. Nuclear magnetic resonance spectra were recorded on a Bruker Avance 400 spectrophotometer operating at 400 MHz for ^1H and 100.61 MHz for ^{13}C , using DMSO- d_6 as solvent and tetramethylsilane

as an internal standard. Chemical shifts (δ) are in ppm, coupling constants (J) are in Hertz (Hz), and the classical abbreviations are used to describe the signal multiplicities. Microanalyses were performed on an Agilent CHNS elemental analyzer and the values are within $\pm 0.4\%$ of the theoretical values. The mass spectrum was obtained on a SHIMADZU-GCMS 2010-DI-2010 spectrometer equipped with a direct inlet probe operating at 70 eV. High-resolution mass spectrum (HRMS) was recorded on an Agilent Technologies Q-TOF 6520 spectrometer *via* electrospray ionization (ESI). The UV-Vis absorption spectrum of **4-OHFPz** was obtained in a solution of acetonitrile at room temperature in the range of 200 to 600 nm with a Shimadzu UV-Vis 160A spectrophotometer.

2.2. Synthesis

2.2.1. Synthesis of 3-*tert*-butyl-1-phenyl-1H-pyrazole-5-amine (**1**)

Compound **1** was synthesized by following reported methodologies [8,9]. Phenylhydrazine (2.1220 g, 19.62 mmol) and 4,4-dimethyl-3-oxopentanenitrile (1.8502 g, 14.78 mmol) were added into a solution of concentrated hydrochloric acid (4 mL) in water (32 mL). The mixture was heated to 70 °C under constant stirring for 1 h. Then, concentrated hydrochloric acid (4 mL) was added and the mixture was further heated for 1 h. The reaction mixture was cooled in an ice bath and the solution was neutralized with ammonium hydroxide, with the formation of a precipitate. The solid formed was filtered under vacuum and washed with water (5 x 50 mL). The starting precursor **1** was obtained in 76.1% yield as a light brown solid. Anal. Calc. for C₁₃H₁₇N₃: C% 72.52, H% 7.96; N% 19.52. Found: C% 72.78, H% 7.65; N% 19.65. IR (KBr, cm⁻¹): ν_{as} NH₂ 3440, ν_{s} NH₂ 3301, $\nu_{\text{C-H}}$ 3062, ν_{as} CH₃ 2962, ν_{s} CH₃ 2869, ν C=N 1623, ν C=C 1565 cm⁻¹, δ_{as} CH₃ 1376, τ C-H 756, ω C=C 698. ¹H NMR (DMSO-*d*₆): δ 1.32 (s, 9H) H-5; 3.74 (s, 2H) NH₂; 5.51 (s, 1H) H-6; 7.30 (t, 1H) H-11; 7.45 (t, 2H) H-10; 7.54 (d, 2H) H-9 ppm. ¹³C NMR (DMSO-*d*₆): δ 30.0 (C-5); 32.4 (C-4); 90.4 (C-6); 122.1 (C-9); 124.9 (C-10); 144.7 (C-8); 144.8 (C-11); 145.4 (C-7); 164.0 (C-3) ppm. The atoms were numbered according to (Supp. Inf. S1).

2.2.2. Synthesis of the title compound **4-OHFPz**

A mixture of the aminopyrazole **1** (352.46 mg, 1.64 mmol), 4-hydroxybenzaldehyde (200 mg, 1.64 mmol) and glacial acetic acid (5 drops) was stirred for 10 min at room temperature. After reaction was complete (monitored by TLC), the crude solid formed was washed with cold water (5x20 mL) and filtered under vacuum to dryness, affording compound **4-OHFPz** as a beige solid in 97% yield. Single-crystals of compound **4-OHFPz** suitable for X-ray diffraction were grown by slow evaporation of an acetone solution at room temperature. The synthetic procedure for **4-OHFPz** is shown in Scheme 1.

Insert Scheme 1.

Anal. Calc. for C₂₀H₂₁N₃O: C% 75.17, H% 6.52, N% 13.28. Found: C% 75.21, H% 6.63, N% 13.16. M.p: 155.3 °C. MS (70 eV) *m/z* (%) 319 (*M*⁺, 83.43), 304 (*M*⁺-15, 100), 262 (*M*⁺-57, 3.49), 226 (*M*⁺-93, 5.39), 77 (23.29), 57 (13.54). IR (KBr, cm⁻¹): ν O-H 3455.98, ν C-H 3124.27 (pyrazole), ν C-H 3058.7 (aromatic), ν_{as} -CH₃ 2962.27, ν_s -CH₃ 2865.84, ν -C=N 1618.06. ¹H NMR (DMSO-*d*₆): δ 1.34 (s, 9H, *t*Bu-H, H-18); 6.48 (s, 1H, H-15); 6.90 (d, 2H, ³*J* = 8.39 Hz, H-6); 7.33 (t, 1H, ³*J* = 7.41 Hz, H-11); 7.50 (t, 2H, ³*J* = 7.61 Hz, H-10); 7.75 (bd, 4H, H-5 and H-9); 8.76 (s, 1H, H-7); 10.28 (bs, 1H, H-1). ¹³C NMR (DMSO-*d*₆): δ 30.69 (*t*BuC, C-18); 32.66 (C-17); 90.91 (C-15); 116.40 (C-6); 123.86 (C-9); 126.51 (C-11); 127.61 (C-4); 129.09 (C-10); 131.49 (C-5); 140.00 (C-8); 151.01 (C-14); 161.46 (C-7); 161.69 (C-16); 161.77 (C-1). The atoms were numbered according to figure 1.

2.3. X-ray crystal structure determination

Crystal data for **4-OHFPz** were deposited at CCDC with the reference number CCDC 1549505. Single-crystal X-ray data for **4-OHFPz** were collected at 143 K on a Bruker APEX-II CCD diffractometer using MoK α radiation (0.71073 Å) monochromated by graphite. Cell determination and final cell parameters were obtained on all reflections using the Bruker SAINT software included in APEX2 software suite [10]. Data integration and scaling was carried out by using the Bruker SAINT software [11].

The structures were solved by SHELXS-2013 software and then refined by SHELXL-2013 [12], included in WinGX [13] and Olex2 [14]. Non-hydrogen atoms of the molecules were clearly resolved and their full-matrix least-squares refinement with anisotropic thermal parameters was conducted. All hydrogen atoms were stereochemically positioned and refined by the riding model [12]. Hydrogen atoms of the water molecules were localized and fixed (with $U_{iso}(H) = 1.5 \text{ \AA}^2$) on the density map. ORTEP diagram was prepared with Diamond program [15]. TOPOS [16], Mercury [17], and Diamond [15] programs were used in the preparation of the artwork of the polyhedral and topological representations.

3. Computational study

Molecular optimization, harmonic vibration frequency, NMR and energy studies were calculated by *ab-initio* computational methods, such as Hartree-Fock (HF) and DFT, using the hybrid of the functional density B3LYP and B3PW91 with the basis set 6-311G++(d,p) and the Gaussian packet 09 [18] without any obstacle to geometry. Theoretical vibrational spectra of **4-OHFPz** were interpreted by means of Potential Energy Distributions (PED) using the VEDA 4 program [19] and the percentage contribution of the frontier orbitals at each transition of electronic absorption spectrum using GaussSum software [20].

4. Results and discussion

4.1. Structural description.

Details of data collection and refinement are summarized in Table 1. The ORTEP diagram for **4-OHFPz** is shown in Figure 1.

Insert Table 1.

Insert Figure 1.

Compound **4-OHFPz** crystallized in the monoclinic space group P21/n with one molecule per asymmetric unit. This compound is formed by three groups around the pyrazole ring: (i) one phenolamine group, which presents a torsion angle between the rings C3-C4-C14-N2 = $42.44(3)^\circ$; (ii), one phenyl group with a torsion angle C12-C13-N2-N3 = $43.72(3)^\circ$, and

finally, (iii) a *tert*-butyl group (Table 1). A general search in the CCDC database [21] for similar compounds formed from a three substituted pyrazole ring reveals 20 entries of which 3 hits present a good agreement with the obtained compound **4-OHFPz**. VAGYOS [22] and VIKTAM [23] compounds present a similar arrangement around its pyrazole ring, substituted by a phenolamine, a phenyl and a *tert*-butyl groups. These structures present significantly differences in the torsion angles of the substituents (Figure 2), giving to this compound a particular crystallographic arrangement. The compound MEJRAX [24] recently reported, is a structural isomer of **4-OHFPz** with a -OH group in *orto* position. Unlike the compound **2-OHFPz** which present intramolecular O-H \cdots N, the compound **4-OHFPz** have this accessible group enable to form intermolecular interactions. Differences in the OH position provokes structural and supramolecular changes as will be explained below.

Insert Figure 2.

In this case, the supramolecular structure is formed by the O-H \cdots N interaction between the phenol group and one nitrogen atom of the pyrazole ring with a distance of 2.883(3) Å, forming chains along [010] direction (Figure 3 a). The chains are joined by C-H \cdots O and C-H \cdots π interactions with distances 3.612(3) and 3.591(4) Å along [100] and [001] directions, respectively (Figure 3 b and c).

Insert Figure 3.

Another way to observe and quantify the supramolecular interactions is through the Hirshfeld surface [25] and the finger print plots [26]. On the superfice of the Figure 4a, is possible to observe in red colour, the region susceptible to form interactions or hydrogen acceptor groups. As it was expected, the red regions are mainly targered on the OH, N and CH groups involved in the intermolecular interaction. The contribution of each interaction to the formation of the supramolecular structure are obtained from the fingerprint plots, being the most important present in the Figure 4b.

Insert Figure 4.

4.2. Molecular Geometry

Optimization of the geometry in the ground state was carried out by using the HF, B3PW91, and B3LYP levels with the basis set 6-311G++ (d,p). Optimization of the structures is presented in Figure 5. The geometric data obtained are given in Table 2, compared to the experimental data.

Insert Figure 5.

Insert Table 2.

Experimental bond lengths C12-N3, C6-O1, and N4-N5 are observed at 1.277(3), 1.357(2), and 1.370(2) Å, respectively; 1.257, 1.344, and 1.345 Å for the HF level; 1.282, 1.357, and 1.346 Å for the B3PW91 level; and 1.283, 1.364, and 1.355 Å for the B3LYP level. In **4-OHFPz**, the experimental bond C6-O1 (1.357(2) Å) is a typical single bond that is slightly longer than the calculated values in all methods. The experimental bond length of C12=N3 (1.277(3) Å) is in good agreement with the theoretical data of 1.257 Å HF, 1.282 Å B3PW91 and 1.283 Å B3LYP. This result agrees with data reported by Wang *et al.*, [27]. Experimental bond N4-N5 (1.370(2) Å) is a typical N-N single bond [28], consistent with the theoretical data of 1.345 Å HF, 1.346 Å B3PW91, and 1.355 Å B3LYP. Experimental bond C14-N3 (1.387(3) Å) is longer than C14-N4 (1.363(3) Å); this is because the substituent groups are different [29].

Few differences exist between bond lengths (less than 0.16 Å) and calculated angles (less than 3 degrees). By examining the dihedral angles, the differences are more significant mainly in the rotation of the *tert*-butyl group, given that the differences between the atoms involved oscillate between 1 and 60°, for example, the dihedral angle between C30-C29-C28-N5 has a difference of 60° with respect to the methods employed by HF, B3PW91, and B3LYP, which is due to the rotation of the *tert*-butyl group with the pyrazole nitrogen. These results are supported by the structural superposition of the calculated and experimental molecules (Figure 6). From this superposition, it is possible to calculate a RMSD value, which is a measure of the degree of agreement between the experimental and

calculated models. The obtained values show good agreement between experimental and calculated models with values around 0.1 and 0.3.

Insert Figure 6.

4.3. Vibrational analysis

Table 3 shows the list of wave numbers of the bands observed in the FT-IR spectra of **4-OHFPz**. The theoretical frequencies and intensities of the IR spectra were calculated *via* the HF, B3PW91, and B3LYP methods. Usually, scale factors are inputs to change the calculated frequency values. In our calculations, we introduced different scaling factors, 0.899748 for HF, 0.957562 for B3PW91, and 0.960461 for B3LYP.

Insert Table 3.

The experimental FT-IR spectrum is shown in Supp. Inf. S2 and those calculated in Supp. Inf. S3. Discrepancies between the calculated and experimental vibrational frequencies are due to two fundamental reasons: first, the experimental frequencies correspond to the solid phase of KBr and the calculated frequencies belong to the gas phase. Second, the calculation has been made for an isolated molecule in the gas phase and the experimental values include intermolecular interactions. This is the reason why a correction of calculated frequencies is employed using a scaling factor for all HF, B3PW91, and B3LYP methods [30].

4.3.1. O-H and C-OH Vibrations

The OH group provides two normal vibrations, $\nu(\text{O-H})$ and $\nu(\text{C-O})$ [31]. A free hydroxyl group gives frequencies in the range of 3450-3700 cm^{-1} [32]. The OH-bond vibration is observed in the experimental IR spectrum at 3455.98 cm^{-1} and in the calculated values at 3760.95 cm^{-1} for HF, 3721.99 cm^{-1} for B3PW91, 3677.60 cm^{-1} for B3LYP. In addition, the PED analysis shows that this vibration frequency is a pure mode with 100% contribution. Binil *et al.*, [31] reported the vibration of the C-OH bond for [4-butyl-1-(4-hydroxyphenyl)-2-phenyl-3,5-pyrazolydinedione] at 1211 cm^{-1} ; this vibration is observed in the

experimental IR at 1241.99 cm^{-1} , which is consistent with the calculated values observed at 1250.65 cm^{-1} for HF, 1251.90 cm^{-1} for B3PW91, and 1239.95 cm^{-1} for B3LYP. For paracetamol $\nu(\text{C-O})$ was reported at 1240 cm^{-1} [33].

4.3.2. C-H Vibrations

The vibration frequency of the pyrazole C-H bond is observed in the experimental spectrum at 3124 cm^{-1} and in the calculated values at 3059 cm^{-1} for HF, 3149 cm^{-1} for B3PW91 and 3133 cm^{-1} for B3LYP. The PED for this signal is 99%, which shows that the signal was assigned correctly.

In aromatic molecules, the C-H stretching vibrations appear in the range of $3100\text{-}3000\text{ cm}^{-1}$ [32]. In our studies, the experimental frequency of aromatic C-H stretching appears at 3058.7 cm^{-1} . These frequencies appear in the calculated values at 3032.15 cm^{-1} for HF, 3106.64 cm^{-1} for B3PW91 and 3029.29 cm^{-1} for B3LYP.

The aliphatic C-H groups appear below 3000 cm^{-1} [34]. Asymmetric C-H stretching vibration of the *tert*-butyl group was experimentally observed at 2962.27 cm^{-1} and for the theoretical values at 2924.18 cm^{-1} (HF); 2985.30 cm^{-1} (B3PW91); 2960.14 cm^{-1} (B3LYP). The symmetrical C-H stretching vibration was experimentally observed at 2865.84 cm^{-1} and at the theoretical values at 2843.20 cm^{-1} (HF); 2915.96 cm^{-1} (B3PW91); 2899.63 cm^{-1} (B3LYP).

The symmetrical deformations [35] of the methyl groups appear in the $1380 \pm 20\text{ cm}^{-1}$ region. For **4-OHFPz**, the symmetrical deformation of the methyl groups is observed experimentally at 1357.71 cm^{-1} , for the theoretical values are observed at 1394.60 cm^{-1} for HF, 1338.57 cm^{-1} for B3PW91, and 1335.04 cm^{-1} for B3LYP.

The substitution patterns of the aromatic rings can be identified by flexing out of the plane of the C-H bond in the range of $900\text{-}675\text{ cm}^{-1}$ [32]. The characteristic vibrations of *para*-substituted aromatic rings have been observed at 838 cm^{-1} in the experimental IR, 863.75 cm^{-1} for HF, 857.01 cm^{-1} for B3PW91, and 859.61 cm^{-1} for B3LYP.

4.3.3. C-C Vibrations

Generally, bands C=C have varying intensities and are observed at $1650\text{-}1430\text{ cm}^{-1}$ [36]. In our studies, experimental aromatic C=C stretching vibrations were observed at 1527.42 ,

1500.42, and 1448.35 cm^{-1} ; for the calculated values, these appear at 1610.55, 1511.58, and 1421.60 cm^{-1} for HF; 1589.91, 1546.58, and 1425.24 cm^{-1} for B3PW91; 1577.07, 1568.43, and 1430.13 cm^{-1} for B3LYP, the experimental data agree with the theoretical values.

4.3.4. C=N and N=N Vibrations

The most characteristic band of the Schiff base derivatives is a vibration of the C=N bond in the 1500-1700 cm^{-1} region [37]. In our studies, this vibration is observed experimentally at 1618.06 cm^{-1} , which is congruent with that reported by Wang *et al.*, [27]. The theoretical values calculated for the C=N bond are observed at 1682.53 cm^{-1} for HF, 1633.25 cm^{-1} for B3PW91, and 1603.01 cm^{-1} for B3LYP.

All imine compounds exhibit N-C stretching in the 1000-1350 cm^{-1} region [37]. In the experimental IR is observed a band at 1141.71 cm^{-1} , which is attributed to N-C stretching. The calculated values show 1196.66 cm^{-1} for HF, 1147.89 cm^{-1} for B3PW91, and 1196.73 cm^{-1} for B3LYP. Temel *et al.*, [38] reported N-C stretching at 1184 cm^{-1} for the Schiff base (*E*)-2-nitro-4-[(phenyl-imino)methylphenol], which is consistent with our results.

The experimental N-N stretching band of the pyrazole ring was observed at 1141 cm^{-1} , and were calculated at 1196.66 cm^{-1} for HF, 1147.89 cm^{-1} for B3PW91, and 1196.73 for B3LYP. For N-N stretching vibration, the results are in good agreement with the similar compounds [39,40].

To see the similarity between experimental and theoretical values, frequencies were plotted in correlation graphs. As shown in Supp. Inf. S4, the value of R^2 is very close to 1.00, therefore, it can be stated that little variation exists in the results and the behavior of the experimental vibrations can be corroborated by both computational methods.

In the correlation graphs, the vibration of the hydroxyl group was not taken into account because it presents a high deviation between the experimental values and the theoretical values. The difference between these values arises as a result of the calculations which not consider the interaction generated between the nitrogen atom of the pyrazole ring on the phenol group, generating a relatively strong intramolecular hydrogen bond.

4.4. NMR studies

The chemical shifts of ^1H and ^{13}C NMR were calculated with *ab initio* and DFT through the GIAO method [41,42] from the optimized geometries, with tetramethylsilane (TMS) as standard and DMSO as solvent. The experimental and theoretical ^1H and ^{13}C chemical shifts in DMSO- d_6 solution are collected in Table 4 (the atoms were numbered according to Figure 5). The experimental ^1H and ^{13}C NMR spectra of the studied molecule are shown in Supp. Inf. S5 and Supp. Inf. S6 respectively. The correlation coefficient (R^2) of ^1H NMR chemical shifts is 0.9926 for HF, 0.9950 for B3PW91 and 0.9924 for B3LYP (Supp. Inf. S7), and (R^2) of ^{13}C NMR chemical shifts is 0.9959 for HF, 0.9981 for B3PW91 and 0.9974 for B3LYP (Supp. Inf. S8).

Insert Table 4.

4.4.1. ^1H NMR

Experimental and calculated chemical shifts of **4-OHFPz** are presented in Table 4. In the ^1H NMR spectrum of the title compound appears 8 signals that integrate for twenty one protons. The NMR chemical shifts of aromatic protons of organic molecules are usually observed in the range of 7.00–8.00 ppm, in the experimental ^1H NMR spectrum, chemical shifts in aromatic protons were observed between 6.9 and 7.75 ppm, while those calculated were obtained between 6.55 and 8.26 ppm (HF); 7.34 and 8.58 ppm (B3PW91); 6.90 and 8.39 ppm (B3LYP). The values calculated are higher and have different values compared to the experimental value; this may be due to the effects of the DMSO solvent. It was observed that the highest deviation in the experimental chemical shift from the values calculated ($\delta_{\text{exp}} - \delta_{\text{theo}}$) was 6.22 ppm (H-2) with HF. The differences with the B3PW91 level were 5.31 ppm (H-2) and 5.41 ppm (H-2) for B3LYP. This can be attributed to the overestimated paramagnetic contribution in the DFT calculations (B3PW91 and B3LYP) [43], given that having a higher level of theory better describes the electronegativity effect and the low field displacement of said atom, otherwise it happens with *ab initio* (HF) calculation, because having a lower level of theory does not take into account the electronegativity effect.

4.4.2. ^{13}C NRM

Fourteen signals for eighteen carbon atoms are observed in the experimental ^{13}C NMR spectrum of **4-OHFPz**. The aromatic carbons give signals in the overlapped areas of the spectrum with chemical shift values from 100 to 150 ppm [44,45]. Similarly, chemical shifts were observed in the values calculated between 151.52 and 104.09 ppm (HF), 161.74 and 115.13 ppm (B3PW91), 167.25 and 119.04 ppm (B3LYP). Due to the effect of an electron-withdrawing group, the chemical shift will be at low field, therefore, it was observed that the deviations of the chemical displacements calculated respect to the experimental ones in the C-6 and C-15 ($\delta_{\text{exp}}-\delta_{\text{teo}}$) carbons were 7.25 ppm (HF), 0.03 ppm (B3PW91) and 5.48 ppm (B3LYP) for C-6, due to the electronegativity property of the oxygen atom. Deviations for the C-15 atom were 4.91 ppm for HF, 1.39 ppm for B3PW91 and 6.62 ppm for B3LYP due to the electronegativity property of the nitrogen atom. In general, the experimental results of ^1H and ^{13}C NMR with the level DFT / 6-311G++ (d, p) represent a better approximation to the data observed experimentally.

4.5. *Electronic properties*

The time-dependent density functional theory (TD-DFT) method is used to calculate the UV-Vis spectrum. In addition, electron-absorption spectra were calculated using the Time-Dependent Self-Consistent Field (TD-SCF) method by using the optimized structure with the base set 6-311G++(d,p) in acetonitrile as solvent.

Insert Figure 7.

The experimental UV-Vis spectrum for **4-OHFPz** (See Figure 7) shows four absorption bands at 197 nm ($\epsilon = 74700 \text{ L mol}^{-1} \text{ cm}^{-1}$) 234 nm ($\epsilon = 44683 \text{ L mol}^{-1} \text{ cm}^{-1}$), 298 nm ($\epsilon = 36640 \text{ L mol}^{-1} \text{ cm}^{-1}$) and 334 nm ($\epsilon = 46518 \text{ L mol}^{-1} \text{ cm}^{-1}$) in CH_3CN . The absorption bands at 197, 234 and 298 nm are assigned to $\pi \rightarrow \pi^*$ transition associated to the aromatic rings (pyrazole and phenyl) and the band at 334 nm is assigned to $\pi \rightarrow \pi^*$ transition within the C=N azomethine group [32].

Insert Table 5.

The experimental UV-Vis spectrum shows four different possible transitions, with a maximum absorption at 334, 298, 234 and 197 nm, respectively. From the calculated values

(See Table 5), three transitions appear at 258.31, 221.95, and 219.45 nm for HF; 353.02, 321.21, and 292.77 nm for B3PW91; and 355.15, 324.53, and 293.57 nm for B3LYP in the gas phase. The oscillator strength for the respective theoretical transitions are 0.7915, 0.0164, and 0.0106 for HF; 0.8065, 0.1054, and 0.1080 for B3PW91; and 0.8050, 0.1019, and 0.0983 for B3LYP.

(A) The band observed at 334 nm was compared to the theoretical data 258.32 nm (HF), 353.02 nm (B3PW91) and 355.15 nm (B3LYP). The strength of the oscillator for the theoretical values were 0.7915 (HF), 0.8065 (B3PW91) and 0.8050 (B3LYP). The band was classified as a possible HOMO \rightarrow LUMO transition with a contribution percentage of 96%.

(B) The band observed at 298 nm was compared to the theoretical data 221.95 nm (HF), 321.21 nm (B3PW91) and 324.53 nm (B3LYP). The strength of the oscillator for the theoretical values were 0.0164 (HF), 0.1054 (B3PW91) and 0.1019 (B3LYP). The band was classified as a possible HOMO-1 \rightarrow LUMO transition with a contribution percentage of 96%.

(C) The band observed at 234 nm was compared to the theoretical data 219.45 nm (HF), 292.77 nm (B3PW91) and 293.57 nm (B3LYP). The oscillator strength for the theoretical values were 0.0106 (HF), 0.1080 (B3PW91) and 0.0983 (B3LYP). The band was classified as a possible HOMO-2 \rightarrow LUMO transition with a contribution percentage of 62%.

The frontier molecular orbitals HOMO and LUMO play a key role in the study of electrical and optical properties. The highest occupied molecular orbital (HOMO) and the lowest unoccupied molecular orbital (LUMO) can determine how the molecule interacts with other species [46]. The HOMO represents the ability to donate an electron, and the LUMO to accept an electron [47]. The difference in energy of a frontier orbital allows characterizing the chemical reactivity and stability of the molecule. A molecule with a small difference in the orbital energy is generally more reactive [48]. That is, a small interval between HOMO-LUMO implies low kinetic stability and high chemical reactivity, as it is energetically favorable to add electrons to a high LUMO and to extract electrons from a low HOMO. Among many other uses, the energy difference between HOMO and LUMO has been used

to predict the activity and intramolecular charge transfer in organic molecules with conjugated π bonds [49,50].

Insert Figure 8.

From Fig. 8a, 8b, and 8c, it can be seen that HOMO is evenly distributed in the central segment and on the phenol and pyrazole rings; whereas LUMO (Figure 8b, 8c) is distributed similarly to HOMO, except that its distribution is partial in the pyrazole ring. The HOMO-1 is distributed over the pyrazole and phenyl rings and partially over the *tert*-butyl group (Figure 8a, 8b, 8c). The LUMO+1 shows an increase in the distribution on the phenol and phenyl rings. This orbital also shows a partial distribution on the pyrazole ring and a null distribution in the *tert*-butyl group. The LUMO and LUMO+1 (8a) show null distribution throughout the molecule, which agrees with the pyrazole electron donor capacity.

4.6. Molecular electrostatic potential (MEP)

The molecular electrostatic potential (MEP) was investigated through HF and DFT theoretical calculations at the 6-311G++ (d,p) level. The MEP is related to the electronic density and it is a very useful descriptor in understanding sites for electrophilic attack and nucleophilic reactions, as well as hydrogen bonding interactions, also it provides a visual method to understand the relative polarity of the molecule [51]. The different values of the electrostatic potential at the surface are represented by different colors; red represents regions of highest electronegative electrostatic potential; blue represents regions of the most positive electrostatic potential; and green represents a region of zero potential. Potential decreases in the red > orange > yellow > green > blue order [52]. Negative regions are usually associated with the lone pair of electronegative atoms [53]. As seen from the MEP of the title molecule (Figure 9) for all methods, regions with negative potential are over the electronegative atoms (oxygen atom of the hydroxy group and nitrogen atom of the pyrazole). Thus, it can be predicted that a metal would preferentially attack **4-OHFPz** at the N-5 position.

Insert Figure 9.

4.7. Global reactivity descriptors

The energy difference between HOMO and LUMO is an important chemical stability index. A small HOMO-LUMO gap automatically means small excitation energies to the manifold of excited states and a large HOMO-LUMO gap implies high stability with respect to chemical reaction [54]. The HOMO and LUMO energies, energy gap (ΔE), ionization potential (IP), electron affinity (EA), absolute electronegativity (χ), absolute hardness (η), absolute softness (σ), chemical potential (μ), and electrophilicity index (ω) for **4-OHFPz** have been calculated at HF, B3PW91 and B3LYP/6-311G++ (d,p) basis set (Figure 8) and the results are given the Table 6.

Insert Table 6.

According to Koopmans' theorem [55] ionization potential (IP) and electron affinity (EA) can be expressed through HOMO and LUMO orbital energies: Ionization potential (IP) = $-E_{\text{HOMO}}$, Electron affinity (EA) = $-E_{\text{LUMO}}$.

The electronegativity (χ), defined by Mulliken [56] as the average of (IP) and (EA):

$$\chi = \frac{IP + EA}{2}$$

The hardness of a molecule is related to the gap between the HOMO and LUMO orbitals. The larger the HOMO-LUMO energy gap the harder the molecule will be [57]. Chemical hardness can be calculated as follows:

$$\eta = \frac{IP - EA}{2}$$

Global softness is the inverse of global hardness [58]:

$$\sigma = \frac{1}{\eta}$$

The electron affinity in combination with ionization energy can also yield chemical potential (μ) defined by Parr and Pearson [59] as the characteristic of molecule electronegativity:

$$\mu = \frac{-(IP + EA)}{2}$$

Parr *et al.*, [60] have introduced the global electrophilicity index (ω) which measures the propensity of a species to accept electrons. It can be calculated by using the electronic chemical potential (μ) and chemical hardness (η):

$$\omega = \frac{\mu^2}{2\eta}$$

The small η value is an indicator of the dominance of the electron donating group in the molecular system. μ is known by an opposite behavior to that of η , so the high value of this parameter is also an indicator of electron donor groups [61].

The frontier orbital energy gaps ($E_{\text{HOMO}}-E_{\text{LUMO}}$) of **4-OHFPz** are found to be 9.3789 eV for HF, 3.9257 eV for B3PW91 and 3.9103 eV for B3LYP in the gas phase. The global softness of the molecule is 0.2132 eV for HF, 0.5094 eV for B3PW91 and 0.5114 eV for B3LYP whereas hardness is 4.6894 eV for HF, 1.9628 eV for B3PW91 and 1.9551 eV for B3LYP which indicate the molecule is relatively hard so it tends to undergo changes or reactions easily. Considering, the chemical hardness, a large HOMO–LUMO gap means a hard molecule and small HOMO–LUMO gap means a soft molecule. One can also relate the stability of the molecule to hardness, which means that the molecule the smallest HOMO–LUMO gap means it is more reactive [62]. GAUSSIAN 09 [18] has been used to construct the shapes of frontier molecular orbitals.

4.8. Non Linear optical (NLO) property study by computational method

Quantum chemical calculations have been shown to be useful in the explanation of the relationship between the electronic structure of the systems and its nonlinear optical properties [63]. Urea is one of the prototypical molecules used in the study of the NLO properties of molecular systems. Therefore it has been used frequently as a threshold value for comparative purposes [64]. The calculations of the total molecular dipole moment (μ), linear polarizability (α) and first-order hyperpolarizability (β) were calculated by DFT/B3LYP method with 6-311G++ (d,p) basis sets using Gaussian 09 program package.

Insert Table 7.

The total molecular dipole moment of **4-OHFPz** from B3LYP with 6-311G++(d,p) basis set is collected in Table 7. The total molecular dipole moment of **4-OHFPz** from this basis set is 3.0992D, which is 1,726 times higher than the value of urea ($\mu = 1.3732$ D). Similarly the first order hyperpolarizability of **4-OHFPz** is 3.8298×10^{-30} esu which is 3.458 times higher than the value of urea ($\beta = 0.372 \times 10^{-30}$ esu). Our title molecule with higher dipole moment and hyperpolarizability value than urea shows that the molecule has large NLO optical property. As seen in Table 7, β_{yyz} component is dominated, having a certain dominant component means that there is a significant charge transfer in this direction.

5. Conclusion

4-((3-(*tert*-Butyl)-(1-phenyl)pyrazole-5-yl)imino)methyl)phenol (**4-OHFPz**) was synthesized and characterized through different techniques, like ^1H NMR, ^{13}C NMR, DEPT 135, 2D NMR (HSQC, HMBC), FT-IR, UV-Vis, MS and single-crystal X-ray diffraction. Vibration frequencies were calculated by using the HF and DFT methods (B3LYP and B3PW91) with 6-311G++(d,p) as the basis set. The title molecule was crystallized in the monoclinic space group P21/n with one molecule per asymmetric unit. The data obtained *via* X-ray diffraction and computational calculations indicate that good correlation exists among these data. To predict the reactive sites for electrophilic and nucleophilic attack for the **4-OHFPz** molecule, the MEP at the optimized geometry was calculated.

Acknowledgement

The authors are grateful to Universidad del Valle, Universidad Santiago de Cali and Universidad del Quindío for financial support to project 789, as well as the contribution by Dr. Ruben Toscano, from the Institute of Chemistry at UNAM (Mexico), in the development of the research.

Appendix

Supplementary crystallographic data for this article is available in: [Optimized and experimental geometries, experimental and theoretical FT-IR spectrum, correlation graphic of the calculated and experimental IR and NMR frequencies]. Cambridge Crystallographic information (CCDC 1549505). It can be obtained free of charge via <http://www.ccdc.cam.ac.uk/>.

References

- [1] I. Damljanovic, M. Vukicevic, N. Radulovic, R. Palic, E. Ellmerer, Z. Ratkovic, M.D. Joksovic, R.D. Vukicevic, Synthesis and antimicrobial activity of some new pyrazole derivatives containing a ferrocene unit, *Bioorg. Med. Chem. Lett.* 19 (2009) 1093-1096.
- [2] A.A. Bekhit, H.M.A. Ashour, Y.S.A. Ghany, A.E.A. Bekhit, A. Baraka, Synthesis and biological evaluation of some thiazolyl and thiadiazolyl derivatives of 1H-pyrazole as anti-inflammatory antimicrobial agents, *Eur. J. Med. Chem.* 43 (2008) 456-463.
- [3] P.T. Chovatia, J.D. Akabari, P.K. Kachhadia, P.D. Zalawadia, H.S. Joshi, Synthesis and selective antitubercular and antimicrobial inhibitory activity of 1-acetyl-3,5-diphenyl-4,5-dihydro-(1h)-pyrazole derivatives, *J. Serb. Chem. Soc.* 71 (2006) 713-720.
- [4] M.D. Joksovic, V. Markovic, Z.D. Juranic, T. Stanojkovic, L.S. Jovanovic, I.S. Damljanovic, K.M. Szecsenyi, N. Todorovic, S. Trifunovic, R.D. Vukicevic, Synthesis, characterization and antitumor activity of novel N-substituted α -amino acids containing ferrocenyl pyrazole-moiety, *J. Organomet. Chem.* 694 (2009) 3935-3942.
- [5] P. Rathelot, N. Azas, H. El-Kashef, F. Delmas, C.D. Giorgio, P. Timon-David, J. Maldonado, P. Vanelle, 1,3-Diphenylpyrazoles: synthesis and antiparasitic activities of azomethine derivatives, *Eur. J. Med. Chem.* 37 (2002) 671-679.

- [6] A.I. Hashem, A.S.A. Youssef, K.A. Kandeel, W.S.I. Abou-Elmagd, Conversion of some 2(3*H*)-furanones bearing a pyrazolyl group into other heterocyclic systems with a study of their antiviral activity, *Eur. J. Med. Chem.* 42 (2007) 934-939.
- [7] G. Jia, R. Tiegang, Z. Jinglai, L. Guihui, L. Weijie, Y. Lirong, Crystal structure characterization as well as theoretical study of spectroscopic properties of novel Schiff bases containing pyrazole group, *Spectrochim. Acta Part A Mol. Biomol. Spectrosc.* 95 (2012) 135–142.
- [8] F. Cuenú, R. Abonia, A. Bolaños, A. Cabrera, Synthesis, structural elucidation and catalytic activity toward a model MizorokieHeck C-C coupling reaction of the pyrazolic Tröger's base Pd₄Cl₈(PzTB)₂ complex, *J. Organomet. Chem.* 696 (2011) 1834-1839.
- [9] S. Hernández, F. Cuenú, R. Abonia, A. Cabrera, 3-*tert*-Butyl-1-(3-nitrophenyl)-1*H*-pyrazol-5-amine, *Acta Cryst.* E68 (2012) 3171.
- [10] APEX2; Bruker AXS Inc.: Madison, Wisconsin, USA, (2012).
- [11] SAINT; Bruker AXS Inc.: Madison, Wisconsin, USA, (2012).
- [12] a) G.M. Sheldrick, A short history of SHELX, *Acta Crystallographica Section A.* 64 (2008), 112-122. b) G.M. Sheldrick, SHELXT – Integrated space-group and crystal structure determination, *Acta Cryst.* C71 (2015) 3-8.
- [13] L.J. Farrugia, WinGX and ORTEP for Windows: an update, *J. Appl. Crystallogr.* 45 (2012) 849-854.
- [14] O.V. Dolomanov, L.J. Bourhis, R.J. Gildea, J.A.K. Howard, H. Puschmann, OLEX2: a complete structure solution, refinement and analysis program, *J. Appl. Crystallogr.* 42 (2009) 339-341.
- [15] K. Brandenburg, H. Putz, In DIAMOND, Impact, C., Ed, Crystal Impact: Kreuzherrenstr. Bonn, Germany, 102 (2006) 53227.
- [16] V.A. Blatov, A.P. Shevchenko, D.M Proserpio, Applied topological analysis of crystal structures with the program package ToposPro, *Cryst. Growth Des.* 14 (2014) 3576-3586.
- [17] C.F. Macrae, I.J. Bruno, J.A. Chisholm, P.R. Edgington, P. McCabe, E. Pidcock, L. Rodriguez-Monge, R. Taylor, J. Van De Streek, P.A. Wood, Mercury CSD 2.0 – new features for the visualization and investigation of crystal structures, *J. Appl. Crystallogr.* 41 (2008) 466-470.

- [18] M.J. Frisch, G.W. Trucks, H.B. Schlegel, G.E. Scuseria, M.A. Robb, J.R. Cheeseman, G. Scalmani, V. Barone, B. Mennucci, G.A. Petersson, H. Nakatsuji, M. Caricato, X. Li, H.P. Hratchian, A.F. Izmaylov, J. Bloino, G. Zheng, J.L. Sonnenberg, M. Hada, M. Ehara, K. Toyota, R. Fukuda, J. Hasegawa, M. Ishida, T. Nakajima, Y. Honda, O. Kitao, H. Nakai, T. Vreven, J.A. Montgomery Jr., J.E. Peralta, F. Ogliaro, M. Bearpark, J.J. Heyd, E. Brothers, K.N. Kudin, V.N. Staroverov, T. Keith, R. Kobayashi, J. Normand, K. Raghavachari, A. Rendell, J.C. Burant, S.S. Iyengar, J. Tomasi, M. Cossi, N. Rega, J.M. Millam, M. Klene, J.E. Knox, J.B. Cross, V. Bakken, C. Adamo, J. Jaramillo, R. Gomperts, R.E. Stratmann, O. Yazyev, A.J. Austin, R. Cammi, C. Pomelli, J.W. Ochterski, R.L. Martin, K. Morokuma, V.G. Zakrzewski, G.A. Voth, P. Salvador, J.J. Dannenberg, S. Dapprich, A.D. Daniels, O. Farkas, J.B. Foresman, J.V. Ortiz, J. Cioslowski, D.J. Fox, Gaussian 09, Revision D.01, Gaussian, Inc, Wallingford CT, (2013).
- [19] a) M.H. Jamróz, Vibrational energy distribution analysis (VEDA): Scopes and limitations, *Spectrochim. Acta A* 114 (2013) 220–230.
- [20] M. O'Boyle, A.L. Tenderholt, K.M. Langner, Software News and Updates cclib: A Library for Package-Independent Computational Chemistry Algorithms, *J. Comp. Chem.* 29 (2008) 839–845.
- [21] C.R. Groom, I.J. Bruno, M.P. Lightfoot, S.C. Ward, The Cambridge Structural Database, *Acta Cryst. B* 72 (2016) 171–179.
- [22] J.N. Low, J. Cobo, M. Nogueras, A. Sanchez, E. Rengifo, R. Abonia, 3-*tert*-Butyl-5-[(4-methoxybenzylidene)amino]-1-phenylpyrazole. *Acta Cryst. E* 59 (2003) o250-o252.
- [23] J. Quiroga, D. Pantoja, J. Cobo, C. Glidewell, (*E*)-3-*tert*-Butyl-4-(4-chlorobenzyl)-*N*-(4-chlorobenzylidene)-1-phenyl-1*H*-pyrazol-5-amine: sheets built from π -stacked hydrogen-bonded dimers, *Acta Cryst. C* 69 (2013) 1039-1042.
- [24] R. Moreno-Fuquen, F. Cuenú, J.E. Torres, G. De la Vega, E. Galarza, R. Abonia, A.R. Kennedy, Presence of $\pi \dots \pi$ and C-H... π interactions in the new Schiff base 2-[(*E*)-[(3-*tert*-butyl-1-phenyl-1*H*-pyrazol-5-yl)imino]methyl]phenol: Experimental and DFT computational studies, *J. Mol. Struct.* 1150 (2017) 366-373.
- [25] F. L. Hirshfeld, Bonded-atom fragments for describing molecular charge densities, *Theor. Chim. Acta* 44 (1977) 129–138.

- [26] J. J. McKinnon, M. A. Spackman, A. S. Mitchell, Novel tools for visualizing and exploring intermolecular interactions in molecular crystals, *Acta Cryst. B* **60** (2004) 627–668.
- [27] Y. Wang, Z. Yu, Y. Sun, Y. Wang, L. Lu, Synthesis, vibrational spectral and nonlinear optical studies of *N*-(4-hydroxy-phenyl)-2-hydroxybenzaldehyde-imine: A combined experimental and theoretical investigation, *Spectrochim. Acta Part A Mol. Biomol. Spectrosc.* **79** (2011) 1475–1482.
- [28] K. Carthigayan, S. Xavier, S. Periandy, HOMO–LUMO, UV, NLO, NMR and vibrational analysis of 3-methyl-1-phenylpyrazole using FT-IR, FT-RAMAN FT-NMR spectra and HF-DFT computational methods, *Spectrochim. Acta Part A Mol. Biomol. Spectrosc.* **142** (2015) 350–363.
- [29] H. Ni, Y. Zhang, F. Zhang, J. Zhao, L. Wu, X. Chu, Synthesis, structural characterization and theoretical approach of 3-(2,6-dichlorobenzyl)-5-methyl-*N*-nitro-1,3,5-oxadiazinan-4-imine, *Spectrochim. Acta Part A Mol. Biomol. Spectrosc.* **138** (2015) 648–659.
- [30] V. Karunakaran, V. Balachandran, Experimental and computational study on molecular structure, natural bond orbital and natural hybrid orbital analysis of non-linear optical material *trans*-3-(*o*-hydroxyphenyl-1-phenyl)-2-propen-1-one, *J. Mol. Struct.* **1053** (2013) 66–78.
- [31] P.S. Binil, Y.S. Mary, H.T. Varghese, C.Y. Panicker, M.R. Anoop, T.K. Manojkumar, Infrared and Raman spectroscopic analyses and theoretical computation of 4-butyl-1-(4-hydroxyphenyl)-2-phenyl-3,5-pyrazolidinedione, *Spectrochim. Acta Part A Mol. Biomol. Spectrosc.* **94** (2012) 101–109.
- [32] O. Tamer, N. Dege, D. Avcı, Y. Atalay, I.O. İlhan, M. Çadır, Synthesis, structural and spectroscopic evaluations and nonlinear optical properties of 3,5-bis(4-methoxyphenyl)-4,5-dihydro-1*H*-pyrazole-1-carbothioic O-acid, *Spectrochim. Acta Part A Mol. Biomol. Spectrosc.* **137** (2015) 1387–1396.
- [33] A.S. EI-Shahawy, S.M. Ahmed, N.K. Sayed, INDO/SCF-CI calculations and structural spectroscopic studies of some complexes of 4-hydroxyacetanilide, *Spectrochim. Acta* **66** (2007) 143–152.
- [34] J. Coates, in: R.A. Meyers (Ed.), *Encyclopedia of Analytical Chemistry: Interpretation of Infrared Spectra, A Practical Approach*, John Wiley and Sons, Chichester, (2000).

- [35] N.G.P. Roeges, *A Guide to the Complete Interpretation of the Infrared Spectra of Organic Structures*, Wiley, New York, (1994).
- [36] P. Govindasamy, S. Gunasekaran, G.R. Ramkumaar, Natural bond orbital analysis, electronic structure and vibrational spectral analysis of N-(4-hydroxyl phenyl) acetamide: A density functional theory, *Spectrochim. Acta Part A Mol. Biomol. Spectrosc.* 130 (2014) 621–633.
- [37] D.L. Pavia, G.M. Lampman, G.S. Kriz, J.R. Vyvyan, *Introduction to Spectroscopy: A Guide for Students of Organic Chemistry*, Brooks/Cole Cengage Learning, USA, (2009).
- [38] E. Temel, C. Alasalvar, H. Gokce, A. Guder, C. Albayrak, Y.B. Alpaslan, G. Alpaslan, N. Dilek, DFT calculations, spectroscopy and antioxidant activity studies on (*E*)-2-nitro-4-[(phenylimino)methyl]phenol, *Spectrochim. Acta Part A Mol. Biomol. Spectrosc.* 136 (2015) 534–546.
- [39] Y.S. Mary, C.Y. Panicker, M. Sapnakumari, B. Narayana, B.K. Sarojini, A.A. Al-Saadi, C.V. Alsenoy, J.A. War, H.K. Fun, Molecular structure, FT-IR, Vibrational assignments, HOMO-LUMO analysis and molecular docking study of 1-[5-(4-Bromophenyl)-3-(4-fluorophenyl)-4,5-dihydro-1H-pyrazol-1-yl]ethanone, *Spectrochim. Acta Part A* 136 (2015) 473-482.
- [40] M. Evecen, H. Tanak, F. Tinmaz, N. Dege, I.O. Ilhan, Experimental (XRD, IR and NMR) and theoretical investigations on 1-(2-nitrobenzoyl)3,5-bis(4-methoxyphenyl)-4,5-dihydro-1H-pyrazole, *J. Mol. Struct.* 1126 (2016) 117-126.
- [41] R. Ditchfield, *Molecular Physics: An International Journal at the Interface Between Chemistry and Physics*, *Mol. Phys.* 274 (1974) 789-807.
- [42] K. Wolinski, J.F. Hinton, P. Pulay, Efficient Implementation of the Gauge-Independent Atomic Orbital Method for NMR Chemical Shift Calculations, *J. Am. Chem. Soc.* 112 (1990) 8251-8260.
- [43] S. Muthu, E.E. Porchelvi, Experimental Spectroscopic (FT-IR, FT-Raman, FT-NMR, UV-Visible) and DFT Studies of 1-ethyl-1, 4-dihydro-7-methyl-4-oxo-1,8-naphthyridine-3-carboxylic acids, *Spectrochim. Acta, Part A* 116 (2013) 220-235.
- [44] K. Pihlaja, E. Kleinpeter, *Carbon-13 Chemical Shifts in Structural and Stereochemical Analysis*, VCH Publishers, Deerfield Beach, (1994).

- [45] H.O. Kalinowski, S. Berger, S. Braun, Carbon-13 NMR Spectroscopy, John Wiley & Sons, Chichester, (1988).
- [46] G. Gece, The use of quantum chemical methods in corrosion inhibitor studies, *Corros. Sci.* 50 (2008) 2981-2992.
- [47] K. Fukui, Role of frontier orbitals in chemical reactions, *Science* 218 (1982) 747-754.
- [48] I. Fleming, Frontier Orbitals and Organic Chemical Reactions, John Wiley & Sons, New York, (1976).
- [49] L. Padmaja, C. Ravikumar, D. Sajan, J. Hubert, V.S. Jayakumar, G.R. Pettit. Density functional study on the structural conformations and intramolecular charge transfer from the vibrational spectra of the anticancer drug combretastatin-A2, *J. Raman Spectrosc.* 40 (2009) 419-428.
- [50] C. Ravikumar, I.H. Joe, V.S. Jayakumar, Charge transfer interactions and nonlinear optical properties of push-pull chromophore benzaldehyde phenylhydrazone: A vibrational approach, *Chem. Phys. Lett.* 460 (2008) 552-558.
- [51] J. Zevallos, A. Toro-Labbe, A theoretical analysis of the Kohn-Sham and Hartree-Fock orbitals and their use in the determination of electronic properties, *J. Chil. Chem. Soc.* 48 (2003) 39-47.
- [52] M. Ozdemir, M. Sonmez, F. Sen, M. Dincer, N. Ozdemir, A novel one-pot synthesis of heterocyclic compound (4-benzoyl-5-phenyl-2-(pyridin-2-yl)-3,3a-dihydropyrazolo[1,5-c]pyrimidin-7(6H)-one): Structural (X-ray and DFT) and spectroscopic (FT-IR, NMR, UV-Vis and Mass) characterization Studies, *Spectrochim. Acta, Part A* 137 (2015) 1304-1314.
- [53] V. Balachandran, M. Murugan, V. Karpagam, M. Karnan, G. Ilango, Conformational stability, spectroscopic (FT-IR & FT-Raman), HOMO-LUMO, NBO and thermodynamic function of 4-(trifluoromethoxy) phenol, *Spectrochim. Acta, Part A* 130 (2014) 367-375.
- [54] J.M.F. Custodio, E.C.M. Faria, L.O. Sallum, V.S. Duarte, W.F. Vaz, G.L.B. De Aquino, P.S. Carvalho Jr, H.B. Napolitano, The Influence of Methoxy and Ethoxy Groups on Supramolecular Arrangement of Two Methoxy-chalcones, *J. Braz. Chem. Soc.* 00 (2017) 1-12.
- [55] T. Koopmans, About the assignment of wave functions and equities to the individual electronics of an atomic, *Physica* 1 (1934) 104-113.

- [56] R.S. Mulliken, A New Electroaffinity Scale; Together with Data on Valence States and on Valence Ionization Potentials and Electron Affinities, *J. Chem. Phys.* 2 (1934) 782-793.
- [57] R.G. Pearson, Absolute Electronegativity and Absolute Hardness of Lewis Acids and Bases, *J. Am. Chem. Soc.* 107 (1985) 6801-6806.
- [58] W. Yang, R.G. Parr, Hardness, softness, and the Fukui function in the electronic theory of metals and catalysis, *Proc. Natl. Acad. Sci. USA.* 82 (1985) 6723-6726.
- [59] R.G. Parr, R.G. Pearson, Absolute Hardness: Companion Parameter to Absolute Electronegativity, *J. Am. Chem. Soc.* 105 (1983) 7512-7516.
- [60] R.G. Parr, L. Szentpaly, S. Liu, Electrophilicity Index, *J. Am. Chem. Soc.* 121 (1999) 1922-1924.
- [61] O. Tamer, B.S. Arslan, D. Avcı, M. Nebiöglu, Y. Atalay, B. Cosut, Synthesis, molecular structure, spectral analysis and nonlinear optical studies on 4-(4-bromophenyl)-1-*tert*-butyl-3-methyl-1H-pyrazol-5-amine: A combined experimental and DFT approach, *J. Mol. Struct.* 1106 (2016) 89-97.
- [62] S. Muthu, S. Renuga, Molecular orbital studies (hardness, chemical potential, electronegativity and electrophilicity), vibrational spectroscopic investigation and normal coordinate analysis of 5-{1-hydroxy-2-[(propan-2-yl)amino]ethyl}benzene-1,3-diol, *Spectrochim. Acta Part A Mol. Biomol. Spectrosc.* 118 (2014) 683-694.
- [63] D.M. Burland, R.D. Miller, C.A. Walsh, Second-order nonlinearity in poled-polymer systems, *Chem. Rev.* 94 (1994) 31-75.
- [64] S. Demir, F. Tinmaz, N. Dege, I.O. İlhan, Vibrational Spectroscopic Studies, NMR, HOMO-LUMO, NLO and NBO analysis of 1-(2-nitrobenzoyl)-3,5-diphenyl-4,5-dihydro-1H-pyrazole with use X-ray Diffractions and DFT calculations, *J. Mol. Struct.* 1108 (2016) 637-648.

TABLES.

Table 1. Crystallographic data and refinement parameters for **4-OHFPz**.

Compound	4-OHFPz
Emp. Formula	C ₂₀ H ₂₁ N ₃ O
FW (g/mol)	319.4
Temp. (K)	298
λ (Å)	0.71073
Crystal system	Monoclinic
Space Group	P21/n
Unit cell	
a (Å)	11.530(3)
b (Å)	12.717(4)
c (Å)	12.327(3)
α(°)	90
β(°)	103.890(5)
γ(°)	90
Volume (Å³)	1754.5(8)
Z	4
ρ calcd (mg/m³)	1.209
Abs.Coeff (mm⁻¹)	0.076
F(000)	680
θ range (°)	2.17 to 27.10
Reflections collected	27019 / 3866
Unique [R(int)]	[0.0604]
Completeness (%)	99
Data / restraints	3866 / 0 /
/ parameters	223
Gof on F²	1.029
R1 [I>2σ(I)]	0.0579
wR2[I>2σ(I)]	0.1410

Table 2. Optimized and experimental geometries of 4-OHFPz in the ground state.

Parameters ^a	Experimental (Δ^*)	HF/6-311++G (d,p) (Δ^*)	B3PW91/6-311++G (d,p) (Δ^*)	B3LYP/6-311++G (d,p) (Δ^*)
Bond Lengths (Å)				
N(5)-N(4)	1.370 (2)	1.345 (25)	1.346 (24)	1.355 (15)
C(6)-O(1)	1.357 (2)	1.344 (13)	1.357 (0)	1.364 (7)
C(7)-C(6)	1.384 (3)	1.391 (7)	1.399 (15)	1.401 (17)
H(8)-C(7)	0.930	1.077	1.087	1.086
C(9)-C(7)	1.370 (3)	1.378 (8)	1.383 (13)	1.385 (15)
H(10)-C(9)	0.931	1.074	1.084	1.083
C(11)-C(9)	1.388 (3)	1.393 (5)	1.402 (14)	1.405 (17)
C(12)-N(3)	1.277 (3)	1.257 (20)	1.282 (5)	1.283 (6)
H(13)-C(12)	0.930	1.086	1.098	1.097
C(14)-N(4)	1.363 (3)	1.350 (13)	1.373 (10)	1.377 (14)
C(14)-N(3)	1.387 (3)	1.386 (1)	1.373 (14)	1.377 (10)
C(15)-N(4)	1.426 (3)	1.418 (8)	1.417 (9)	1.423 (3)
C(16)-C(15)	1.373 (3)	1.385 (12)	1.394 (21)	1.396 (23)
H(17)-C(16)	0.930	1.072	1.082	1.080
C(18)-C(16)	1.381 (3)	1.385 (4)	1.391 (10)	1.393 (12)
H(19)-C(18)	0.930	1.075	1.085	1.084
C(20)-C(18)	1.363 (4)	1.384 (21)	1.391 (28)	1.393 (30)
H(21)-C(20)	0.930	1.075	1.085	1.084
C(22)-C(6)	1.386 (3)	1.386 (0)	1.394 (8)	1.396 (10)
H(23)-C(22)	0.930	1.074	1.084	1.083
C(24)-C(22)	1.378 (3)	1.381 (3)	1.385 (7)	1.387 (9)
H(25)-C(24)	0.930	1.077	1.086	1.085
C(26)-C(14)	1.372 (3)	1.368 (4)	1.390 (18)	1.392 (20)
H(27)-C(26)	0.930	1.069	1.078	1.077
C(28)-N(5)	1.335 (3)	1.298 (37)	1.332 (3)	1.334 (1)
C(29)-C(28)	1.509 (3)	1.518 (9)	1.515 (6)	1.521 (12)
C(30)-C(29)	1.510 (4)	1.539 (29)	1.538 (28)	1.545 (35)
H(31)-C(30)	0.961	1.087	1.095	1.095
H(32)-C(30)	0.960	1.086	1.094	1.094
H(33)-C(30)	0.960	1.086	1.092	1.091
C(34)-C(29)	1.515 (4)	1.539 (24)	1.532 (17)	1.539 (24)
H(35)-C(34)	0.960	1.086	1.094	1.094
H(36)-C(34)	0.960	1.086	1.094	1.094
H(37)-C(34)	0.960	1.087	1.094	1.094
C(38)-C(29)	1.497 (4)	1.534 (37)	1.538 (41)	1.544 (47)
H(39)-C(38)	0.960	1.084	1.094	1.094
H(40)-C(38)	0.960	1.087	1.095	1.095

H(41)-C(38)	0.960	1.084	1.092	1.092
C(42)-C(20)	1.371 (4)	1.386 (15)	1.392 (21)	1.395 (24)
H(43)-C(42)	0.930	1.075	1.085	1.084
C(44)-C(15)	1.374 (3)	1.383 (9)	1.388 (14)	1.391 (17)
H(45)-C(44)	0.930	1.073	1.083	1.082
Bond angles (°)				
C(7)-C(6)-O(1)	122.70 (2)	122.21	122.45	122.47
C(9)-C(7)-C(6)	119.91 (2)	119.92	120.06	120.03
H(8)-C(7)-C(6)	120.0	119.99	119.85	119.85
H(10)-C(9)-C(7)	119.12	120.19	120.64	120.52
C(11)-C(9)-C(7)	121.72 (19)	120.66	120.67	120.69
H(13)-C(12)-N(3)	119.35	121.49	121.68	121.64
C(14)-N(4)-N(3)	119.45 (19)	30.15	29.84	29.83
C(16)-C(15)-N(4)	119.93 (19)	121.03	121.17	121.16
H(17)-C(16)-C(15)	119.92	120.10	119.97	120.00
C(18)-C(16)-C(15)	120.20 (2)	119.72	119.49	119.55
H(19)-C(18)-C(16)	120.13	119.38	119.28	119.29
C(20)-C(18)-C(16)	119.70 (3)	120.48	120.60	120.59
H(21)-C(20)-C(18)	119.81	120.26	120.24	120.25
C(22)-C(6)-O(1)	117.93 (18)	117.59	117.50	117.42
H(23)-C(22)-C(6)	119.90	119.28	119.08	119.11
C(24)-C(22)-C(6)	120.10 (2)	119.29	119.45	119.43
H(25)-C(24)-C(22)	119.43	118.98	119.28	119.26
C(26)-C(14)-N(4)	106.77 (18)	106.96	105.89	105.97
H(27)-C(26)-C(14)	127.08	126.94	126.49	126.39
C(28)-N(5)-N(4)	105.10 (16)	106.74	106.12	106.16
C(29)-C(28)-N(5)	121.03 (19)	122.12	119.80	119.85
C(30)-C(29)-C(28)	108.12 (2)	109.05	109.11	109.21
H(31)-C(30)-C(29)	109.38	110.31	110.32	110.31
H(32)-C(30)-C(29)	109.50	111.58	110.99	110.97
H(33)-C(30)-C(29)	109.51	110.89	111.69	110.74
C(34)-C(29)-C(28)	110.40 (2)	109.12	110.43	110.49
H(35)-C(34)-C(29)	109.38	110.94	111.59	111.59
H(36)-C(34)-C(29)	109.41	111.67	111.54	111.55
H(37)-C(34)-C(29)	109.46	110.26	109.89	109.89
C(38)-C(29)-C(28)	110.73 (2)	110.77	109.16	109.25
H(39)-C(38)-C(29)	109.43	111.33	111.01	110.99
H(40)-C(38)-C(29)	109.46	109.60	110.33	110.31
H(41)-C(38)-C(29)	109.52	111.36	110.68	110.74
C(42)-C(20)-C(18)	120.21 (3)	119.48	119.51	119.49
H(43)-C(42)-C(20)	119.69	120.11	120.13	120.12
C(44)-C(15)-N(4)	119.80 (2)	118.85	118.58	118.66

H(45)-C(44)-C(15)	120.41	120.87	121.33	121.19
Dihedral angles (°)				
H(8)-C(7)-C(6)-O(1)	2.17	-0.04	-0.13	-0.12
C(9)-C(7)-C(6)-O(1)	-177.82	-179.92	-179.88	-179.87
H(10)-C(9)-C(7)-C(6)	178.41	179.88	179.65	179.66
C(11)-C(9)-C(7)-C(6)	-1.57	-0.07	-0.17	-0.18
H(17)-C(16)-C(15)-N(4)	-0.85	0.04	0.13	-0.005
C(18)-C(16)-C(15)-N(4)	179.33	179.68	179.71	179.67
H(19)-C(18)-C(16)-C(15)	179.19	179.98	-179.91	-179.91
C(20)-C(18)-C(16)-C(15)	-0.94	-0.85	-0.89	-0.84
H(21)-C(20)-C(18)-C(16)	-179.95	-179.55	-179.55	-179.57
C(22)-C(6)-O(1)-C(7)	179.78	-179.95	-179.88	-179.90
H(23)-C(22)-C(6)-O(1)	-1.74	-0.02	-0.02	-0.02
C(24)-C(22)-C(6)-O(1)	178.30	179.96	179.95	179.95
H(25)-C(24)-C(22)-C(6)	-179.43	179.99	179.96	179.97
C(26)-C(14)-N(4)-N(3)	173.90	176.27	175.65	175.76
H(27)-C(26)-C(14)-N(4)	-179.32	-176.76	-177.36	-177.43
C(29)-C(28)-N(5)-N(4)	-177.55	-179.78	-179.98	-179.99
C(30)-C(29)-C(28)-N(5)	90.073	119.03	59.38	59.39
H(31)-C(30)-C(29)-C(28)	-172.33	179.77	-178.86	-178.96
H(32)-C(30)-C(29)-C(28)	67.73	59.92	61.26	61.20
H(33)-C(30)-C(29)-C(28)	-52.38	-60.44	-58.64	-58.72
C(34)-C(29)-C(28)-N(5)	-150.61	-121.54	179.65	179.64
H(35)-C(34)-C(29)-C(28)	58.65	60.31	60.85	60.79
H(36)-C(34)-C(29)-C(28)	-61.34	-60.10	-60.46	-60.49
H(37)-C(34)-C(29)-C(28)	178.65	-179.92	-179.79	-179.85
C(38)-C(29)-C(28)-N(5)	-0.30	-1.22	-60.09	-60.14
H(40)-C(38)-C(29)-C(28)	178.19	179.83	179.18	179.33
H(41)-C(38)-C(29)-C(28)	58.20	59.85	59.09	59.19
C(42)-C(20)-C(18)-C(16)	0.07	0.067	-0.01	0.01
H(43)-C(42)-C(20)-C(18)	-179.09	-179.75	-179.72	-179.75
H(45)-C(44)-C(15)-N(4)	1.59	0.39	0.37	0.37
H(45)-C(44)-C(42)-C(20)	178.92	-179.87	-179.83	-179.81

Table 3. Assignments of vibrational wavenumbers by VEDA 4 (cm^{-1}) for **4-OHFPz**.

Assignments	Experimental	6-311++G(d,p)								
		HF			DFT B3PW91			DFT B3LYP		
		%(PED)	Frequency	Intensity	%(PED)	Frequency	Intensity	%(PED)	Frequency	Intensity
vOH	3455.98	100	3760.95	140.39	100	3692.35	113.80	100	3677.60	109.76
vC26-H27	3124.27	99	3059.14	1.29	99	3149.97	0.27	100	3133.02	0.34
vCHRing	3058.7	96	3032.15	32.78	96	3106.64	22.38	97	3029.29	25.08
vasCH3	2964.2	97	2924.18	100.35	94	2985.30	96.29	95	2960.14	104.66
vsCH3	2865.84	96	2843.20	64.88	96	2915.96	35.67	90	2899.63	39.94
vC12-N3	1618.06	50	1682.53	478.56	67	1633.25	221.08	65	1603.01	279.60
vC6-C7	1527.42	30	1610.55	260.79	47	1589.91	243.12	56	1577.07	122.07
vC15-C44	1500.42	15	1511.58	198.24	44	1546.58	184.86	64	1568.43	164.12
vC7-C9	1448.35	32	1421.60	76.63	37	1425.24	70.04	13	1430.13	56.13
δ CH3	1363.71	53	1394.60	74.34	50	1338.57	19.22	76	1335.04	12.30
δ H2-O1-C6	1272.85	42	1295.64	7.04	21	1277.90	8.65	11	1309.11	14.33
vO1-C6	1241.99	60	1250.65	184.59	58	1251.90	231.87	40	1239.95	239.77
vN4-N5	1141.71	23	1196.66	15.33	39	1147.89	40.31	25	1196.73	50.02
δ C14-N4-N5	1018.28	14	1083.12	31.94	21	1037.68	10.22	27	1037.42	19.29
τ H8-C7-C9-H10	991.28	78	989.72	6.97	83	965.89	21.29	56	963.34	27.99
δ H8-C7-C9	838.92	17	863.75	63.63	17	857.01	16.11	15	859.61	14.69
τ H8-C7-C9-C11	804.21	87	818.77	12.87	84	792.55	10.87	64	807.75	12.78
δ H17-C16-C18	754.07	36	674.80	32.63	38	676.03	28.35	31	678.08	34.96
τ H2-O1-C6-C7	688.85	62	692.80	3.38	64	697.21	3.13	50	522.49	5.93
δ H17-C16-C15	592.07	26	611.83	20.51	59	601.87	29.25	43	608.93	24.86
δ H8-C7-C6	511.07	43	510.85	3.82	23	534.15	21.34	11	537.78	20.73
δ H2-O1-C6	472.50	33	466.86	1.84	23	479.20	3.05	19	481.27	3.68

τ H17-C16-C18-H19	443.57	81	457.87	0.44	32	476.35	6.97	37	476.62	6.39
δ H2-O1-C6	-	27	367.89	0.14	20	364.79	11.78	26	390.82	1.61

ν , stretching; δ , bending; τ , torsion; s, symmetric; as, asymmetric. Potential Energy Distribution (PED).

Table 4. NMR theoretical (δ_{Theo}) and experimental (δ_{Exp}) shifts for **4-OHFPz**.

Atom	Experimental	DFT/6-311++G (d,p)		
		HF	B3PW91	B3LYP
2-H	10.28	4.06	4.97	4.87
13-H	8.76	8.55	8.99	8.86
10-H	7.75	8.26	8.58	8.39
25-H	7.75	7.76	7.93	7.75
45-H	7.75	7.69	8.28	8.14
17-H	7.75	7.15	8.01	7.81
43-H	7.48	7.48	7.92	7.76
19-H	7.48	7.33	7.88	7.72
21-H	7.31	7.28	7.76	7.58
23-H	6.90	6.83	7.34	7.19
8-H	6.90	6.55	7.04	6.90
27-H	6.48	5.58	6.59	6.43
39-H	1.34	1.05	1.27	1.16
41-H	1.34	0.99	1.89	1.77
36-H	1.34	0.98	1.59	1.47
32-H	1.34	0.97	1.20	1.09
37-H	1.34	0.67	1.21	1.10
31-H	1.34	0.65	1.22	1.11
35-H	1.34	0.58	1.59	1.47
33-H	1.34	0.55	1.82	1.66
40-H	1.34	0.47	1.27	1.17
6-C	161.77	154.52	161.74	167.25
28-C	161.69	158.33	163.36	169.21
12-C	161.46	159.13	158.65	162.19
14-C	151.01	147.71	150.46	156.28
15-C	140.00	135.09	141.39	146.62
24-C	131.49	133.44	136.67	140.83
9-C	131.49	127.44	129.38	133.30
42-C	129.09	122.77	129.59	133.54
18-C	129.09	121.80	128.61	132.56
11-C	127.61	116.65	129.40	134.75
20-C	126.51	119.28	126.85	130.91
16-C	123.86	119.06	126.01	130.13
44-C	123.86	118.37	124.04	128.26
22-C	116.40	104.46	115.13	119.04
7-C	116.40	104.09	115.46	119.34
26-C	90.91	76.21	89.76	92.0

29-C	32.66	18.29	32.45	37.73
30-C	30.69	16.86	28.04	31.68
34-C	30.69	16.19	24.32	28.09
38-C	30.69	12.75	27.98	31.67

ACCEPTED MANUSCRIPT

Table 5. Experimental and theoretical electronic absorption wavelengths and important contributions for **4-OHFPz**.

Exp.	HF				DFT							
					B3LYP				B3PW91			
λ	λ	E	f	Important contributions	λ	E	f	Important contributions	λ	E	f	Important contributions
197	-	-	-	-	-	-	-	-	-	-	-	-
234	219	5.6497	0.0106	H-7→L+6 (4%) H-7→L+8 (4%) H-6→L+6 (7%) H-6→L+7 (3%) H-6→L+8 (8%) H-3→L+6 (9%) H-3→L+7 (5%) H-3→L+8 (9%)	293	4.2233	0.0983	H-7→LUMO (3%) H-5→LUMO (23%) H-3→LUMO (3%) H-2→LUMO (62%)	292	4.2348	0.1010	H-7→LUMO (3%) H-5→LUMO (22%) H-3→LUMO (3%) H-2→LUMO (63%) H-1→LUMO (2%) H→LUMO (2%)
298	221	5.5862	0.0164	H-4→L+6 (9%) H-4→L+7 (5%) H-4→L+8 (10%) H-4→L+13 (2%) H-3→L+17 (2%) H-3→L+18 (7%) H→L+15 (4%) H→L+16 (3%) H→L+17 (10%) H→L+18 (16%)	324	3.8204	0.1019	H-1→LUMO (97%)	321	3.8599	0.1054	H-1→LUMO (96%)
334	258	4.7997	0.7915	H→L+6 (28%) H→L+7 (14%) H→L+8 (28) H→L+10 (3%) H→L+13 (4%)	355	3.4920	0.8050	HOMO→LUMO (96%)	353	3.5121	0.8065	HOMO→LUMO (96%)

λ : wavelength (nm); f : oscillator strength; E: excitation energy (eV)

Table 6. HOMO - LUMO energies and calculated global reactivity parameters of **4-OHFPz** calculated *via* HF, B3PW91 and B3LYP/6-311G++ (d, p) method.

Parameters	HF	B3PW91	B3LYP
E_{HOMO}	-8.3498	-6.0738	-6.0279
E_{LUMO}	1.0291	-2.1481	-2.1176
$\Delta E_{\text{HOMO}} - E_{\text{LUMO}}$	9.3789	3.9257	3.9103
Electronegativity (χ)	3.6603	4.1109	4.0727
Chemical hardness (η)	4.6894	1.9628	1.9551
Global softness (σ)	0.2132	0.5094	0.5114
Electrophilicity index (ω)	1.4285	4.3049	4.2419
Chemical potential (μ)	-3.6603	-4.1109	-4.0727

Table 7. The molecular electric dipole moment μ (Debye), polarizability α ($\times 10^{-24}$ esu) and hyperpolarizability β ($\times 10^{-30}$ esu) values of **4-OHFPz**

Property	B3LYP/6-311++G (d,p)
μ_x	0
μ_y	0
μ_z	3.0992
μ_{tot}	3.0992
α_{xx}	25.7419
α_{xy}	-1.6969
α_{yy}	45.6701
α_{xz}	5.3488
α_{yz}	-0.6306
α_{zz}	62.1581
α_{tot}	44.5234
β_{xxx}	-3.3430
β_{xxy}	-0.3270
β_{xyy}	0.5894
β_{yyy}	0.3024
β_{xxz}	-0.2058
β_{yzx}	-0.6550
β_{yyz}	2.8205
β_{xzz}	1.0736
β_{yzz}	-2.7453
β_{zzz}	-0.5719
β_{tot}	3.8298

FIGURES.

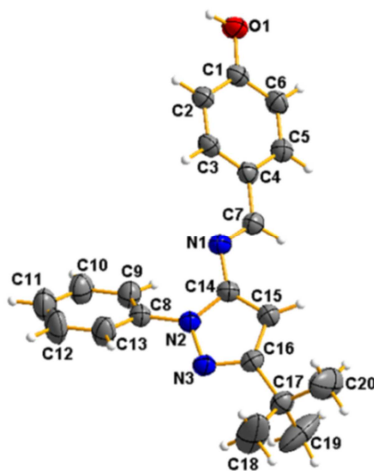


Figure 1. ORTEP diagram showing 50% probability for 4-OHFPz.

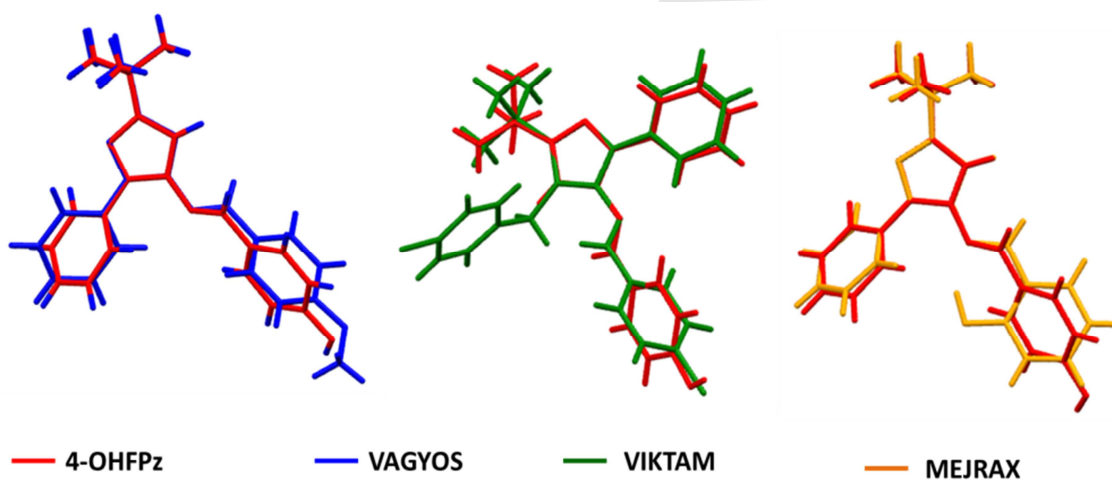


Figure 2. Superposition of 4-OHFPz and previously reported compounds.

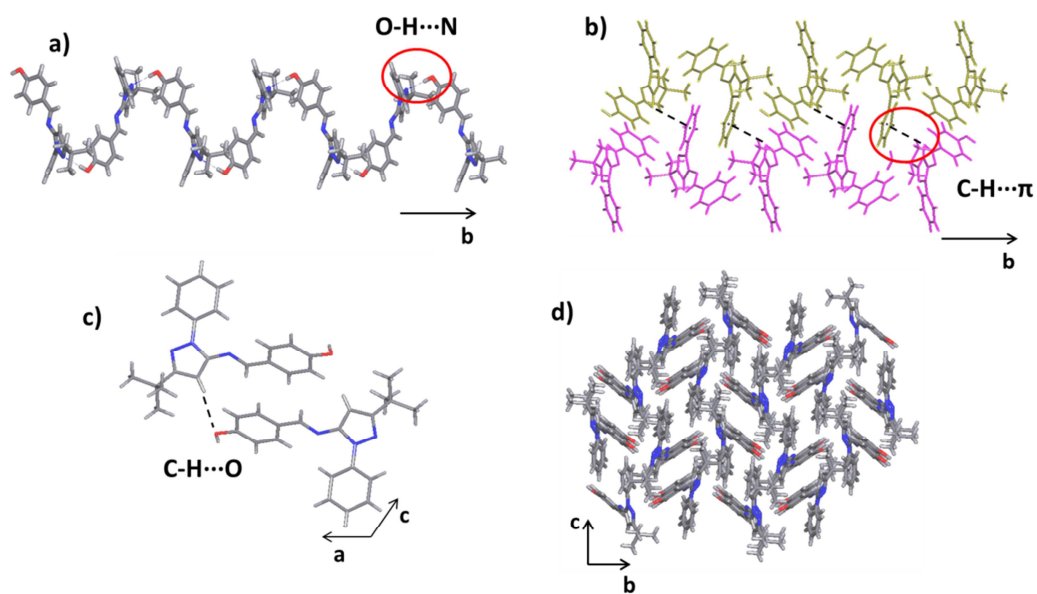


Figure 3. a) Formation of the chains along [010], b) junction of the chains by C-H... π interaction in the plane (110). c) C-H...O interaction along [001] direction to form the 3D supramolecular crystal packing d) view along [100] direction for the compound 4-OHFPz.

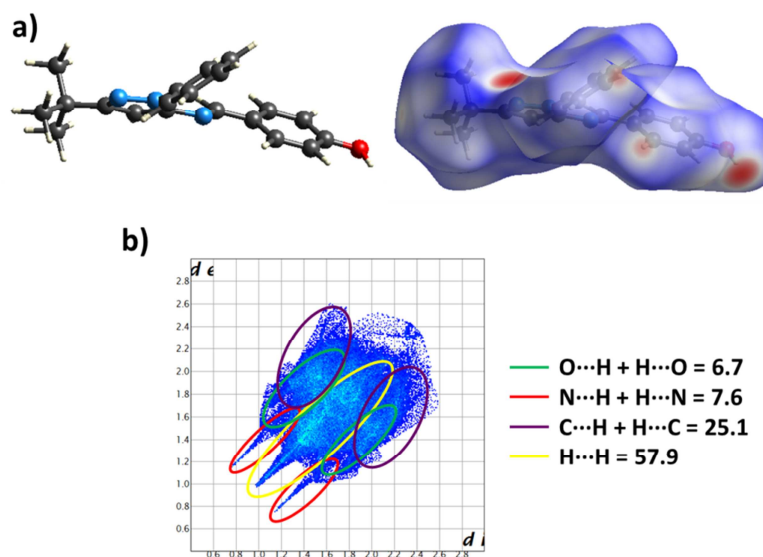


Figure 4. a) d_{norm} Hirshfeld surface and b) fingerprint plot for the compound 4-OHFPz.

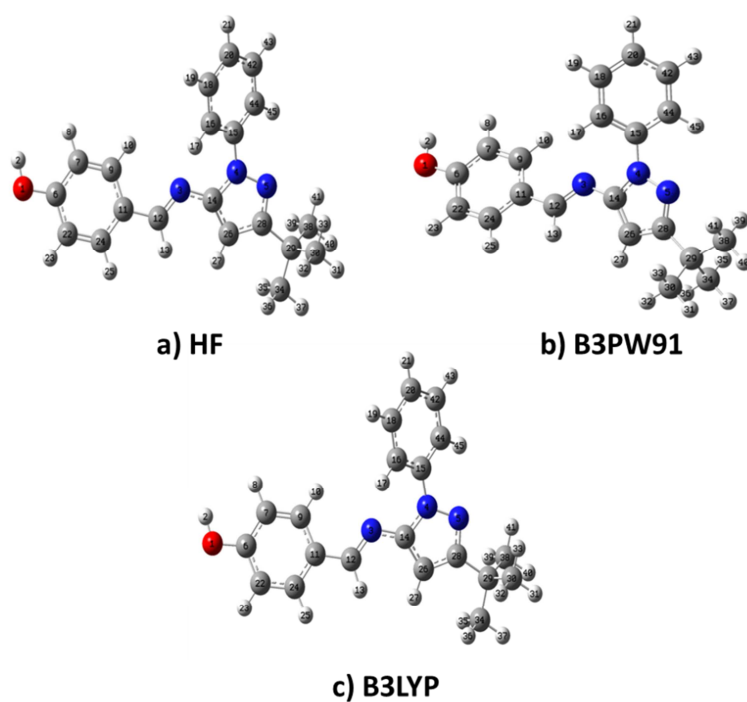


Figure 5. Optimized structures of **4-OHFPz** (a) HF, (b) B3PW91, (c) B3LYP.

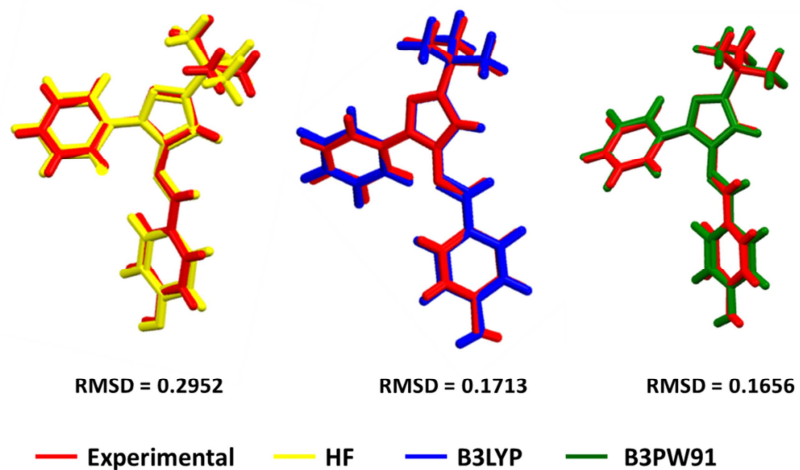


Figure 6. Superposition of the experimental structure measured by single-crystal X-ray diffraction and calculated structures of **4-OHFPz**.

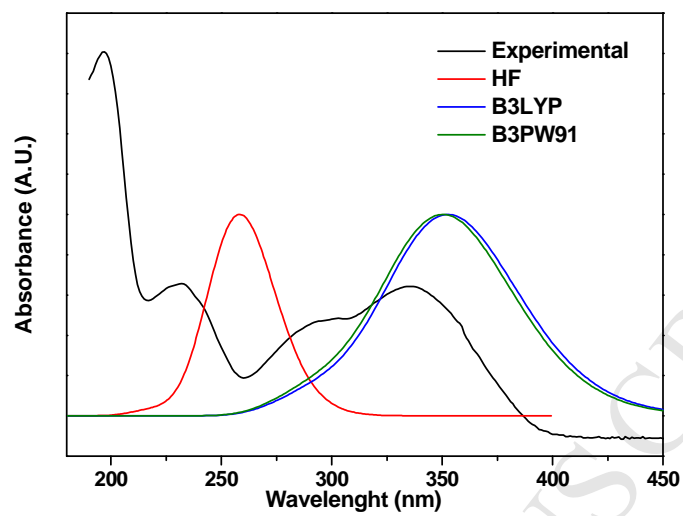


Figure 7. Comparison of experimental and theoretical UV-Vis spectra of **4-OHFPz**. (a) experimental; (b) HF; (c) B3PW91 and (d) B3LYP.

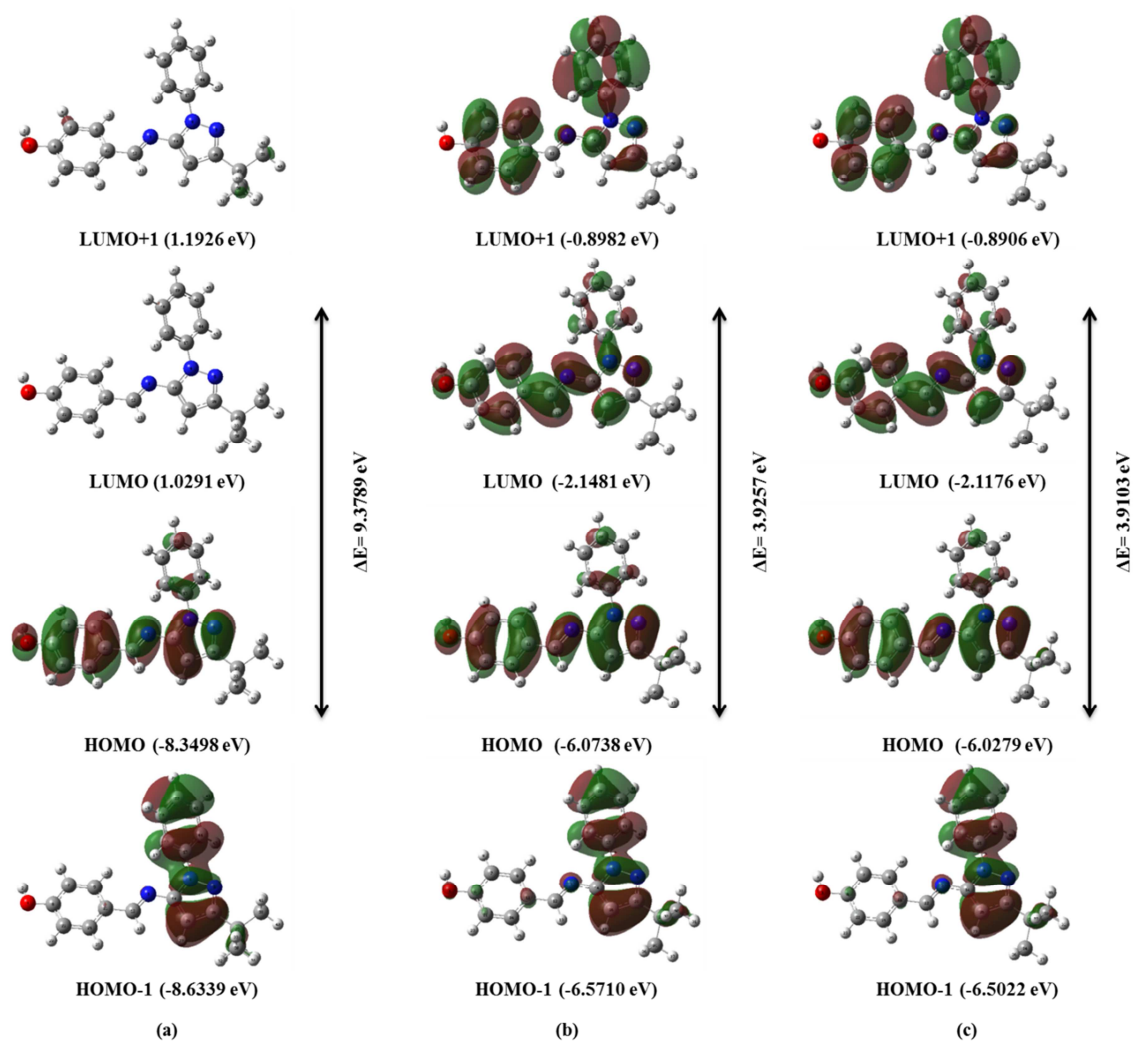


Figure 8. Pictures of occupied and unoccupied MOs obtained at (a) HF, (b) B3PW91 and (c) B3LYP for compound **4-OHFPz**.

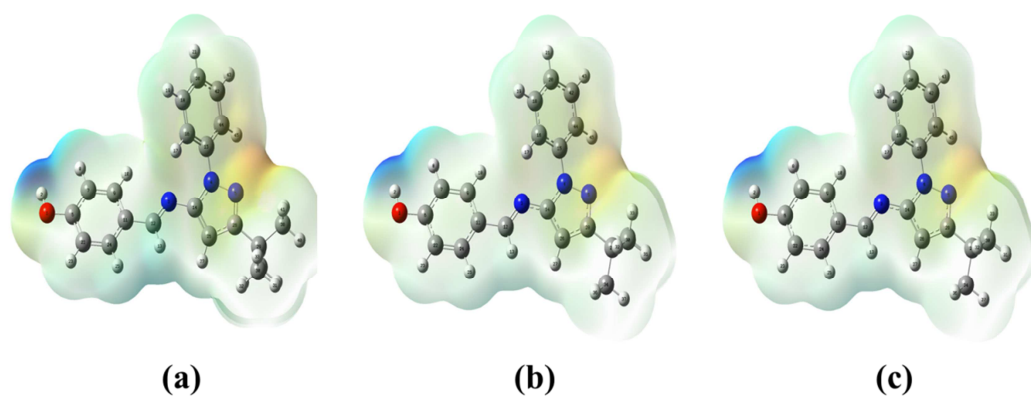
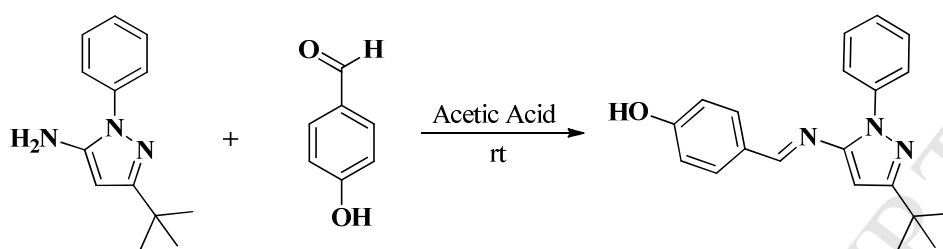


Figure 9. Electrostatic potential surface for compound **4-OHFPz** (a) HF, (b) B3PW91 and (c) B3LYP.

SCHEMES.



Scheme 1. Synthesis of compound 4-OHFPz.

HIGHLIGHTS

- A novel molecule was synthesized.
- X-ray diffraction, FT-IR and NMR were applied to solve molecular structure.
- The DFT theoretical results were compared with the experimental results.
- Polarizability and first hyperpolarizability of the compound were calculated.
- The DFT calculations of the compound, MEP and global reactivity descriptors were also examined.